ASME Journal of Computing and Information Science in Engineering
Online journal at:
https://asmedigitalcollection.asme.org/computingengineering

A Matrix-Based Approach to Unified Synthesis of Planar Four-Bar Mechanisms for Motion Generation With Position, Velocity, and Acceleration Constraints

Xueting Deng
Computer-Aided Design and Innovation Lab,
Department of Mechanical Engineering,
Stony Brook University,
Stony Brook, NY 11794-2300
e-mail: xueting.deng@stonybrook.edu

Anurag Purwar[1]
Computer-Aided Design and Innovation Lab,
Department of Mechanical Engineering,
Stony Brook University,
Stony Brook, NY 11794-2300
e-mail: anurag.purwar@stonybrook.edu

This paper introduces a novel matrix-based approach for the simultaneous type and dimensional synthesis of planar four-bar linkage mechanisms, accommodating various practical constraints, including position, velocity, acceleration, and joint placements. Traditional design processes segregate type synthesis, the determination of joint and link configurations, from dimensional synthesis, which involves specifying link sizes and pivot locations. This segregation often leads to complexities in addressing the complete design challenge. The novel methodology proposed in this paper departs from the conventional sequential design approach by concurrently evaluating type and dimensional parameters using a data-driven matrix formulation. The crux of the paper's methodology involves formulating a singular design equation through a transformation matrix, parameterized by the Cartesian parameters of the mechanism's dyads. This formulation linearly expresses a broad range of constraints, facilitating the identification of viable solutions through singular value decomposition and null space analysis. This integrated approach not only simplifies the synthesis process but also provides direct insights into the mechanism's parameters, encompassing both type and dimensions, thereby obviating the need for further interpretative steps common to the use of quaternions and kinematic mapping. In essence, the paper presents two main contributions: the development of a unified design equation capable of encompassing a wide array of constraints within the mechanism synthesis process, and the introduction of an algorithm that effectively identifies all potential planar four-bar linkage mechanisms by accurately satisfying up to five constraints. This approach promises to enhance the design and optimization of mechanical systems by offering a more holistic and efficient pathway to mechanism synthesis. [DOI: 10.1115/1.4066661]

Keywords: four-bar mechanism, kinematics, motion synthesis, type synthesis, velocity synthesis, acceleration synthesis, computational synthesis, computer-aided design

1 Introduction

Planar four-bar linkage mechanisms are widely acknowledged as the foundational and most comprehensively studied single-degree-of-freedom (DOF) closed-loop mechanisms, well-known for their capacity to generate complex motion patterns and trajectories. These mechanisms are integral to a myriad of ubiquitous devices, including but not limited to, automotive windshield wipers, elliptical exercise machines, exoskeletons, and internal combustion engines. Figure 1 shows two predominant variants of four-bar linkages. The synthesis of such mechanisms entails the specification of joints and links, including number, type, and interconnection pattern (referred to as number and type synthesis), along with the determination of pivot locations and link dimensions (referred to as dimensional synthesis). Type synthesis is often perceived as the more formidable challenge within mechanism design, while dimensional synthesis is systematically categorized into path, motion, and function synthesis. Path synthesis focuses on designing mechanisms that direct a point on a coupler along a predetermined trajectory or follow a few precision points while motion synthesis is concerned with the guided movement of the coupler as a rigid body, and function synthesis aims to delineate the input–output relationship within a mechanism. This paper deals with the simultaneous type and dimensional synthesis of planar four-bar linkages, taking into account various practical geometric and kinematic constraints such as position, velocity, acceleration, and pivot placements. The

[1]Corresponding author.

Manuscript received February 1, 2024; final manuscript received September 16, 2024; published online November 5, 2024. Assoc. Editor: Ekta Singla.

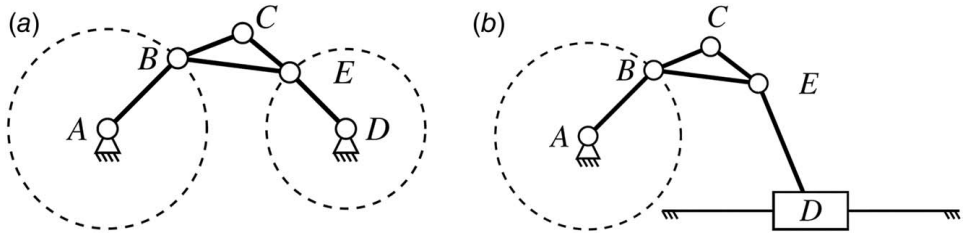

Fig. 1 Two examples of planar four-bar mechanisms with their constituent dyads: (*a*) RR+RR and (*b*) slider-crank (RR+PR), where R and P stand for revolute and prismatic joints, respectively

conventional sequential approach involves presupposing a mechanism type and then deducing dimensional parameters with individual equations for each type. Departing from the conventional sequential approach, this paper introduces a matrix-based methodology that concurrently determines both type and dimensional attributes from given data with one unified design equation.

Quaternions, initially introduced by Hamilton [1], are four-dimensional complex numbers, which have been used for representing rotations in 3D space [2]. Kinematicians have utilized their extension to dual quaternions for representing rigid body displacements in SE(3) [3], and a special case of dual quaternions called planar quaternions are used to represent an element of SE(2). The concept of kinematic mapping has been used to represent rigid body motions as a curve in a higher-dimensional projective space [4]. Ravani and Roth [5,6] laid the foundation for a comprehensive theory of kinematic mapping in both planar and spatial motion synthesis. Subsequent researches by Bottema and Roth [7], Bodduluri and McCarthy [8], McCarthy [9], Larochelle [10,11], and Ge and McCarthy [12,13] further refined and extended this theory to encompass exact and approximate motion synthesis for various types of mechanisms, including planar, spherical, and spatial dyads. It is well-known that the aforementioned methods for motion synthesis are not independent of the location of moving and fixed reference frames, a problem commonly known as bi-invariance [14,15]. Xue et al. [16] recently presented a bi-invariant approach to approximate motion synthesis of planar four-bar linkage mechanisms using pole displacement. McCarthy's book [3] provides a comprehensive introduction to the derivation of constraint equations for dyads and triads of various mechanism types.

The concept of simultaneous type and dimensional synthesis of four-bar mechanisms for exact positions was introduced by Hayes et al. [17,18], who employed heuristics to identify RR and PR dyads, with R and P denoting revolute and prismatic joints, respectively. Building on this foundation, Ge et al. [19] proposed an innovative approach for concurrently determining the type and dimensions of planar four-bar mechanisms. This novel approach transformed the problem of synthesizing four-bar mechanisms into a computational shape analysis problem, with the goal of identifying a pair of constraint manifolds whose intersection contains the image curve. Deshpande and Purwar [20] extended this approach to address a more generalized version of the classic Burmester problem. Subsequently, Purwar et al. [21,22] implemented a motion synthesis algorithm based on kinematic mapping in a web-based mechanism design and simulation software known as MOTIONGEN.[2] Additionally, Zhao et al. [23] extended this approach to address the five-position synthesis problem for planar six-bar mechanisms.

In 1979, Schaefer and Kramer [24] presented precision synthesis by incorporating pose and velocity constraints. Following their work, Holte et al. [25,26] derived equations for approximate position and velocity synthesis. Building on these contributions, Robson et al. [27–29] further extended the problem to encompass velocity and acceleration constraints for both planar and spatial mechanisms. It is worth noting that all of these approaches, while valuable in their own right, are primarily focused on specific mechanism types and do not seek to unify constraints in a manner that simplifies computer implementation or seeks to find all possible solutions to the problem.

This paper presents a novel matrix-based approach, unifying the simultaneous type and dimensional synthesis of planar four-bar mechanisms, while accommodating various constraints encompassing pose, velocity, acceleration, and joint location considerations. This work is built on the foundation given by Ge et al. [19]. However, unlike conventional methods that rely on kinematic mapping and quaternions for synthesis, our approach directly formulates a singular design equation capable of handling a wide array of constraint types. This equation is constructed through a transformation matrix, parameterized by the Cartesian parameters and geometric constraints of the constituent dyads, effectively expressing constraints linearly. Additionally, we extend our approach to incorporate velocity and acceleration constraints, achieved by differentiating with respect to time. The resulting set of geometric and kinematic constraints constitutes a system of linear equations, which is systematically solved using singular value decomposition (SVD). Through a null space analysis of this system, we identify candidate solutions, subject to fundamental constraints governing the Cartesian parameters of the mechanism. Subsequently, we ascertain the dyad types from the derived solutions and perform an inverse kinematic computation to determine the dimensions. Notably, our method offers direct access to mechanism parameters, encapsulating information on both type and dimensions in the Cartesian space, eliminating the need for further interpretation or clarification. In summary, this paper presents two original contributions: (1) a unified design equation has been developed to handle position, velocity, acceleration, and geometric constraints related to both pivots and lines within all categories of planar dyads, and (2) an integrated algorithm has been introduced to accurately meet up to five constraints, thus enabling the identification of all potential planar four-bar linkage mechanisms.

The remainder of this paper is organized as follows. Section 2 provides an overview of four-bar mechanisms and their constituent dyads, outlining their geometric constraints in terms of Cartesian parameters. In Secs. 3 and 4, we delve into the planar transformation and present a unified synthesis equation for all dyads types using the transformation matrix. In Sec. 5, we introduce the singular value decomposition and outline a two-step process for solving the synthesis equations. Finally, in Sec. 6, we illustrate the application of our method through a variety of example problems.

2 Planar Four-Bar Mechanisms and Geometric Constraints

A planar four-bar mechanism is the simplest closed-loop single-DOF mechanism. Formed by two dyads, the motion of the coupler of a planar four-bar mechanism has to satisfy the geometric constraints of both the dyads. There are four different types of dyads: revolute-revolute (RR), prismatic-revolute (PR), revolute-prismatic (RP), and prismatic-prismatic (PP), each consisting of two planar kinematic joints; see Fig. 2. For example, an RRRR mechanism shown in

[2]www.motiongen.io

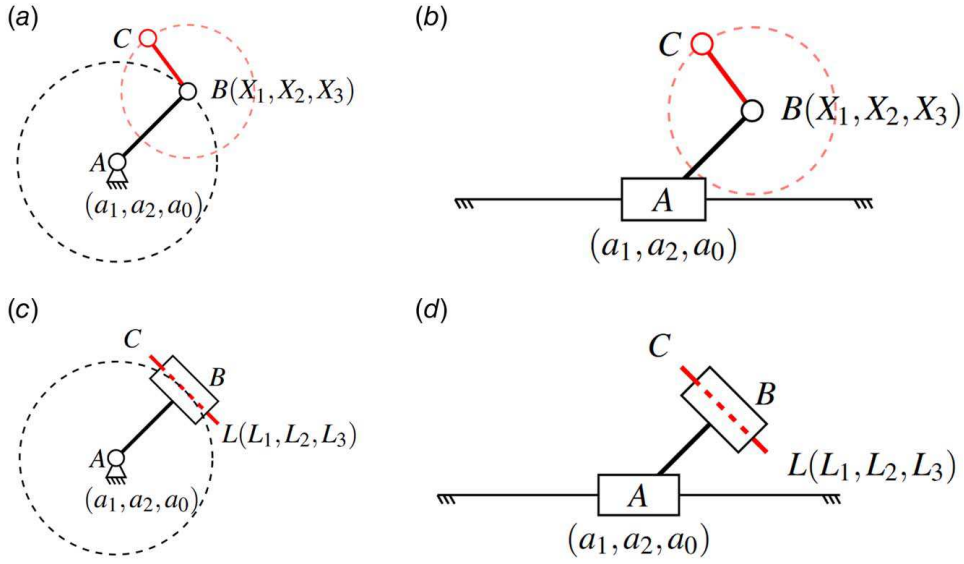

Fig. 2 Planar dyads: (*a*) RR, (*b*) PR, (*c*) RP, and (*d*) PP with point and line coordinates shown using homogeneous coordinates where a_0, X_3, and L_3 are homogenizing factors

Fig. 1 is composed of two RR dyads. The revolute joints B and E rotate around fixed revolute joints A and D, respectively. The coupler $\triangle BCE$ is constrained by both dyads AB and DE, which makes the trajectory of point C complex (a degree-six algebraic curve), but predictable. In the motion synthesis problem, the goal is to find the parameters of dyads that lead the coupler to pass through the given task poses.[3] Likewise, the RRRP mechanism shown in Fig. 1(*b*) is formed by an RR dyad and a PR dyad. In the rest of this section, we present the geometric constraints of all four types of dyads using homogeneous coordinates. The choice of homogeneous coordinates is made to handle degenerate cases gracefully and simplify computation. Moreover, they also enable us to leverage the principle of projective duality to find similar design equations for different types of dyads. We also give the velocity and acceleration constraints equations by differentiating geometric constraints with respect to time.

2.1 Geometric Constraints of Revolute-Revolute and Prismatic-Revolute Dyads. In RR dyads, the motion of the moving pivot is constrained along a circular path, as depicted in Fig. 2(*a*), where pivot B undergoes rotation around the fixed pivot A. Similarly, on link BC, the joint C also follows a circular trajectory centered around the pivot B. In this context, $\boldsymbol{a} + (a_1,\ a_2,\ a_3,\ a_0)$ represents the homogeneous coordinates of the fixed pivot A, where the term a_3 is a function of the radius r of the RR dyad. The affine coordinates of the fixed pivot A are given by $(a_1/a_0,\ a_2/a_0)$. Similarly, $\boldsymbol{X} + (X_1,\ X_2,\ X_3); X_3 \neq 0$ denotes the homogeneous coordinates of the moving pivot B with the affine coordinates as $(X_1/X_3,\ X_2/X_3)$.

As the moving pivot traces a circular trajectory around the fixed pivot, the constraint equation for an RR dyad expressed in affine coordinates is given by

$$\left(\frac{X_1}{X_3} - \frac{a_1}{a_0}\right)^2 + \left(\frac{X_2}{X_3} - \frac{a_2}{a_0}\right)^2 = r^2 \tag{1}$$

which simplifies to

$$a_1X_1 + a_2X_2 + a_3X_3 = a_0\left(\frac{X_1^2 + X_2^2}{2X_3}\right) \tag{2}$$

where a newly introduced parameter a_3 and radius r are related by

$$r^2 = \frac{a_1^2 + a_2^2 + 2a_0a_3}{a_0^2} \tag{3}$$

When $a_0 + 0$, the radius r approaches ∞, degenerating the circle into a line. For the PR dyad shown in Fig. 2(*b*), the slider A slides on a fixed line, where the moving joint B is constrained to move along a line parallel to the fixed line. Thus, a PR dyad can be considered as a special case of an RR dyad.

Equation (1) can be differentiated to obtain constraints on velocity and acceleration as

$$\dot{X}_1\left(\frac{X_1}{X_3} - \frac{a_1}{a_0}\right) + \dot{X}_2\left(\frac{X_2}{X_3} - \frac{a_2}{a_0}\right) + 0 \tag{4}$$

and

$$\ddot{X}_1\left(\frac{X_1}{X_3} - \frac{a_1}{a_0}\right) + \ddot{X}_2\left(\frac{X_2}{X_3} - \frac{a_2}{a_0}\right) + \frac{\dot{X}_1^2}{X_3} + \frac{\dot{X}_2^2}{X_3} + 0 \tag{5}$$

2.2 Geometric Constraints of Revolute-Prismatic and Prismatic-Prismatic Dyads. In an RP dyad shown in Fig. 2(*c*), the geometric constraint is that a line BC stays tangent to a circle. Let the radius of the circle be r. When $r + 0$, the tangent line swings about joint A, which is the typical configuration of a linear actuator or a swinging block rotating about a fixed point. Let $\boldsymbol{L} + (L_1,\ L_2,\ L_3); L_3 \neq 0$ denotes the homogeneous coordinates of a line in the fixed-frame F, with the affine coordinates $(L_1/L_3,\ L_2/L_3)$. The line geometric constraint is given by

$$a_1L_1 + a_2L_2 + a_0L_3 = \pm a_0r\sqrt{L_1^2 + L_2^2} \tag{6}$$

Distinct from the other three dyads, the movement of the PP dyads, shown in Fig. 2(*d*), is characterized by a rectilinear motion, which also makes them less useful in typical motion synthesis applications where a change in orientation is required. According to Ref. [19], the motion of a PP dyad is constrained such that the angle between a line $\boldsymbol{L} + (L_1,\ L_2,\ L_3)$ and another line $(2a_1,\ 2a_2,\ a_3)$ in F is fixed and thus the constraint is given by

$$a_1L_1 + a_2L_2 = 0.5k \tag{7}$$

where k is a constant that corresponds to the angle between the two lines. Thus, Eq. (7) can be considered as a special case of Eq. (6).

[3]In this paper, we use the words pose and positions interchangeably, which describe translation and rotation of a moving frame.

Using the principle of duality, the point constraint given by Eq. (2) and line constraint by Eq. (6) are dual to each other [30,31].

By differentiating Eq. (6) with time t, we obtain velocity and acceleration constraints of RP and PP dyads as

$$a_1\dot{L}_1 + a_2\dot{L}_2 + a_0\dot{L}_3 = \pm a_0 r\frac{L_1\dot{L}_1 + L_2\dot{L}_2}{\sqrt{L_1^2 + L_2^2}} \tag{8}$$

and

$$a_1\ddot{L}_1 + a_2\ddot{L}_2 + a_0\ddot{L}_3 = \pm a_0 r\left(\frac{\dot{L}_1^2 + \dot{L}_2^2 + L_1\ddot{L}_1 + L_2\ddot{L}_2}{\sqrt{L_1^2 + L_2^2}} - \frac{(L_1\dot{L}_1 + L_2\dot{L}_2)^2}{\sqrt{(L_1^2 + L_2^2)^3}}\right) \tag{9}$$

3 Kinematic Representation Using Homogeneous Matrix

In the context of motion synthesis problems, a series of poses is often defined based on their locations and orientations relative to the reference frame F. In Fig. 1, it is essential for the coupler to attain specific target poses. These target poses are attached with moving coordinate systems denoted as M_i. Notably, the moving joint B maintains its position relative to each of these M_i coordinate systems throughout the motion. This inherent characteristic proves to be pivotal in resolving motion synthesis challenges. We establish the requisite design equations by transferring the coordinates of the moving joint from M_i to the reference frame F and subsequently solving for them. The following section elaborates on the transformation process of the moving pivot's coordinates and their derivatives using homogeneous matrices.

Let $\boldsymbol{x} + (x_1,\ x_2,\ x_3)$ represent the coordinates of the moving joint within M_i, and correspondingly, let $\boldsymbol{X} + (X_1,\ X_2,\ X_3)$ denote the coordinates of this joint within the reference frame F. The relationship between $\boldsymbol{X}$ and $\boldsymbol{x}$ is established through a homogeneous matrix transformation given by

$$\boldsymbol{X}^T = [T]\boldsymbol{x}^T \tag{10}$$

where

$$[T] = \begin{bmatrix} \cos\phi & -\sin\phi & d_1 \\ \sin\phi & \cos\phi & d_2 \\ 0 & 0 & 1 \end{bmatrix} \tag{11}$$

In this transform, $\boldsymbol{d} + (d_1,\ d_2)$ and ϕ denote the origin of the moving frame and its orientation in F, respectively, as shown in Fig. 3.

Differentiating Eq. (10) with respect to time t, the velocity and acceleration transformation between F and M are given by Eqs. (12) and (14) with the linear velocity $\boldsymbol{u} + (\dot{d}_1,\ \dot{d}_2) + (v,\ w)$.

$$\dot{\boldsymbol{X}}^T = [\dot{T}]\boldsymbol{x}^T \tag{12}$$

where

$$[\dot{T}] = \begin{bmatrix} -\dot{\phi}\sin\phi & -\dot{\phi}\cos\phi & v \\ \dot{\phi}\cos\phi & -\dot{\phi}\sin\phi & w \\ 0 & 0 & 0 \end{bmatrix} \tag{13}$$

and

$$\ddot{\boldsymbol{X}}^T = [\ddot{T}]\boldsymbol{x}^T \tag{14}$$

where

$$[\ddot{T}] = \begin{bmatrix} -\ddot{\phi}\sin\phi - \dot{\phi}^2\cos\phi & -\ddot{\phi}\cos\phi + \dot{\phi}^2\sin\phi & \dot{v} \\ \ddot{\phi}\cos\phi - \dot{\phi}^2\sin\phi & -\ddot{\phi}\sin\phi - \dot{\phi}^2\cos\phi & \dot{w} \\ 0 & 0 & 0 \end{bmatrix} \tag{15}$$

Similarly, let $\boldsymbol{L} + (L_1,\ L_2,\ L_3)$ and $\boldsymbol{l} + (l_1,\ l_2,\ l_3)$ represent the homogeneous coordinates of a line in F and M, respectively, then using the principle of projective duality [31], Eq. (16) gives the line transformation from the M to F.

$$\boldsymbol{L}^T = [H]\boldsymbol{l}^T \tag{16}$$

where $[H]$ is the transpose of the inverse of matrix $[T]$. Equations (17) and (18) express the velocity and acceleration transformation of a line between F and M as following:

$$\dot{\boldsymbol{L}}^T = [\dot{H}]\boldsymbol{l}^T \tag{17}$$

and

$$\ddot{\boldsymbol{L}}^T = [\ddot{H}]\boldsymbol{l}^T \tag{18}$$

4 A Unified Design Equation

With the geometric constraint and their first- and second-order derivative equations and transformations given in the last two sections, we can now derive design equations for each type of dyads and unify them.

4.1 Design Equations for Revolute-Revolute and Prismatic-Revolute Dyads.

The design equations for RR and PR dyads can be obtained by substituting $\boldsymbol{X}$ from Eq. (10) in Eq. (2) as

$$\begin{aligned} &-a_0x_1^2 - a_0x_2^2 + (-d_1^2 - d_2^2)a_0x_3^2 + 2d_1a_1x_3^2 + 2d_2a_2x_3^2 \\ &+ 2a_3x_3^2 + (-2cd_1 - 2sd_2)a_0x_1x_3 + 2ca_1x_1x_3 + 2sa_2x_1x_3 \\ &+ (2sd_1 - 2cd_2)a_0x_2x_3 - 2sa_1x_2x_3 + 2ca_2x_2x_3 = 0 \end{aligned} \tag{19}$$

where s refers to $\sin\phi$ and c refers to $\cos\phi$. In Eq. (19), the terms s, c, and $\boldsymbol{d} + (d_1,\ d_2)$ are completely known from the given task poses. There are five unknown terms in this equation which are a_1, a_2, a_3, x_1, and x_2 (a_0 and x_3 are homogenizing factors). For n task poses, we obtain n such equations. It is challenging to find a direct solution for cubic equations, such as above with five variables. However, this equation can be decomposed into a bi-linear equation by introducing appropriate intermediate variables. After combining like terms, Eq. (19) can be written as

$$A_1P_1 + A_2P_2 + \cdots + A_8P_8 = 0 \tag{20}$$

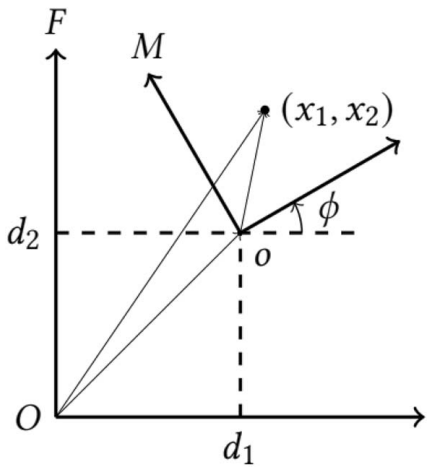

Fig. 3 Planar displacement

where

$$P_1 = a_0x_3, \quad P_2 = 2a_0x_1, \quad P_3 = 2a_0x_2,$$
$$P_4 = 2a_1x_3, \quad P_5 = 2a_2x_3, \quad P_6 = 2a_2x_1 - 2a_1x_2,$$
$$P_7 = 2a_1x_1 = 2a_2x_2, \quad P_8 = (-a_0x_1^2 - a_0x_2^2 + 2a_3x_3^2)/x_3 \tag{21}$$

and

$$A_1 = (-d_1^2 - d_2^2), \quad A_2 = -cd_1 - sd_2,$$
$$A_3 = sd_1 - cd_2, \quad A_4 = d_1, \quad A_5 = d_2,$$
$$A_6 = s, \quad A_7 = c, \quad A_8 = 1 \tag{22}$$

This way, Eq. (20) becomes a linear equation in terms of unknowns P_i for given pose parameters (d_1, d_2, ϕ).

Substituting $\boldsymbol{X}$ and $\dot{\boldsymbol{X}}$ from Eqs. (10) and (12) in Eq. (4) provides the velocity constraint equation for RR and PR dyads, which is in the same form as Eq. (20). The velocity equation has the same set of unknown P_i as given in Eq. (21), but has different A_i as

$$A_1 = d_1v = d_2w, \quad A_2 = \frac{1}{2}(cv + sw - sd_1\dot{\phi} + cd_2\dot{\phi}),$$
$$A_3 = \frac{1}{2}(cw - sv - cd_1\dot{\phi} - sd_2\dot{\phi}), \quad A_4 = -\frac{1}{2}v,$$
$$A_5 = -\frac{1}{2}w, \quad A_6 = -\frac{1}{2}c\dot{\phi}, \quad A_7 = \frac{1}{2}s\dot{\phi}, \quad A_8 = 0 \tag{23}$$

Similarly, the acceleration constraint equation is obtained by substituting $\boldsymbol{X}$, $\dot{\boldsymbol{X}}$, and $\ddot{\boldsymbol{X}}$ from Eq. (14) in Eq. (5). With the same parameter P_i, the A_i parameters for the acceleration are given by

$$A_1 = v^2 + w^2 + d_1\dot{v} + d_2\dot{w},$$
$$A_2 = \frac{1}{2}[c(-d_1\dot{\phi}^2 + d_2\ddot{\phi} + 2\dot{\phi}w + \dot{v}) + s(-d_2\dot{\phi}^2 - d_1\ddot{\phi} - 2\dot{\phi}v + \dot{w})],$$
$$A_3 = \frac{1}{2}[c(-d_2\dot{\phi}^2 - d_1\ddot{\phi} - 2\dot{\phi}v + \dot{w}) + s(d_1\dot{\phi}^2 - d_2\ddot{\phi} - 2\dot{\phi}w - \dot{v})],$$
$$A_4 = -\frac{1}{2}\dot{v}, \quad A_5 = -\frac{1}{2}\dot{w}, \quad A_6 = \frac{1}{2}(-\ddot{\phi}c + \dot{\phi}^2 s),$$
$$A_7 = \frac{1}{2}(\ddot{\phi}s + \dot{\phi}^2 c), \quad A_8 = 0 \tag{24}$$

Since there are only five independent parameters of a dyad, P_i should satisfy two constraints, which turn out to be quadratic

$$2P_1P_6 - P_2P_5 + P_3P_4 = 0$$
$$2P_1P_7 - P_2P_4 - P_3P_5 = 0 \tag{25}$$

For PR dyads, since $a_0 + 0$, we get $P_1 + P_2 + P_3 + 0$. Thus, the quadratic constraints in Eq. (25) are satisfied automatically. In this case, since we have only four independent parameters to determine, at most four constraints can be satisfied exactly. If synthesis reveals this particular pattern or zeros in the P_i, then we can conclude that we have found a PR dyad.

Once the intermediate variable P_i are found, the parameters a_i and x_i can be solved using inverse kinematic equations from Eq. (21) as

$$x_1 : x_2 : x_3 = (P_5P_6 + P_4P_7) : (-P_4P_6 + P_5P_7) : (P_4^2 + P_5^2) \tag{26}$$

and

$$a_0 : a_1 : a_2 : a_3 = 2P_1 : P_4 : P_5 : \left(P_8 + \frac{P_1(P_6^2 + P_7^2)}{P_4^2 + P_5^2}\right) \tag{27}$$

4.2 Design Equations for Revolute-Prismatic and Prismatic-Prismatic Dyads. The design equations of RP and PP dyads can be derived by substituting $\boldsymbol{L}$ from Eq. (16) into Eq. (6). Again, the design equations of RP and PP are in the same form as Eq.(20) and have the same parameters A_i as in Eq.(22). However, the parameters P_i are given by

$$P_1 = 0, \quad P_2 = a_0l_1, \quad P_3 = a_0l_2,$$
$$P_4 = 0, \quad P_5 = 0, \quad P_6 = a_2l_1 - a_1l_2,$$
$$P_7 = a_1l_1 = a_2l_2, \quad P_8 = a_0l_3 \mp a_0r \tag{28}$$

The inverse computation for Cartesian parameters of the dyads are given by

$$l_1 : l_2 : l_3 = P_2 : P_3 : 2P_8 \tag{29}$$

and

$$a_0 : a_1 : a_2 = (P_2^2 + P_3^2) : (P_2P_7 - P_3P_6) : (P_2P_6 + P_3P_7) \tag{30}$$

The intermediate P_i terms for PP dyad are

$$P_1 = 0, \quad P_2 = 0, \quad P_3 = 0,$$
$$P_4 = 0, \quad P_5 = 0, \quad P_6 = a_2l_1 - a_1l_2,$$
$$P_7 = a_1l_1 + a_2l_2, \quad P_8 = -0.5k \tag{31}$$

For P_i of both RP and PP dyads, Eq. (25) is satisfied automatically. For RP dyads, we have $P_1 = P_4 = P_5 = 0$, which automatically satisfies two quadratic conditions. Therefore, the maximum number of the given constraints for exact synthesis tasks for RP dyads is four. Similarly, the fundamental constraint equations for PP dyads are $P_1 = P_2 = P_3 = P_4 = P_5 = 0$. In this paper, we are not concerned with the PP dyads since their geometric constraints do not permit a change in orientation of the moving object.

Considering Eq. (20) as the unified design equation, synthesis of different dyad types can be performed in conjunction with quadratic constraints in Eq. (25). The pattern of zeros in the parameters P_i indicates the type of dyad, viz., RR, RP, and PR. For example, $P_1 = P_2 = P_3 = 0$ encodes a PR dyad, $P_1 = P_4 = P_5 = 0$ encodes an RP dyad, and $P_1 = P_2 = P_3 = P_4 = P_5 = 0$ encodes a PP dyad. In all other cases, it is an RR dyad. Therefore, Eq. (20) is a unified design equation, that is capable of representing both type and dimensions of planar dyads.

Substituting $\dot{\boldsymbol{L}}$ from Eq. (17) in Eq. (8) provides the velocity constraint equation for RP and PP dyads. The velocity equation has the same P_i as in Eq. (28), but has different A_i as following:

$$A_1 = 0, \quad A_2 = -c(d_2\dot{\phi} = v) = s(d_1\dot{\phi} - w),$$
$$A_3 = c(d_1\dot{\phi} - w) = s(d_2\dot{\phi} = v), \quad A_4 = 0,$$
$$A_5 = 0, \quad A_6 = c\dot{\phi}, \quad A_7 = -s\dot{\phi}, \quad A_8 = 0 \tag{32}$$

The acceleration constraint equation is obtained by substituting $\boldsymbol{L}$, $\dot{\boldsymbol{L}}$, and $\ddot{\boldsymbol{L}}$ from Eq. (18) in Eq. (9). With the same parameters P_i as in Eq. (28), the A_i parameters for the acceleration are given by

$$A_1 = 0,$$
$$A_2 = \frac{1}{2}[c(d_1\dot{\phi}^2 - d_2\ddot{\phi} - 2\dot{\phi}w - \dot{v}) + s(d_2\dot{\phi}^2 + d_1\ddot{\phi} + 2\dot{\phi}v - \dot{w})],$$
$$A_3 = \frac{1}{2}[c(d_2\dot{\phi}^2 + d_1\ddot{\phi} + 2\dot{\phi}v - \dot{w}) + s(-d_1\dot{\phi}^2 + d_2\ddot{\phi} + 2\dot{\phi}w + \dot{v})],$$
$$A_4 = 0, \quad A_5 = 0, \quad A_6 = \ddot{\phi}c - \dot{\phi}^2 s,$$
$$A_7 = -\dot{\phi}^2 c - \ddot{\phi}s, \quad A_8 = 0 \tag{33}$$

In summary, Eq. (20) represents the unified design equation, which represents pose-, velocity-, and acceleration constraints on all types of dyads. Moreover, we have derived this equation directly in terms of Cartesian parameters, which are readily interpretable.

Fig. 4 Human ankle poses during a typical walking gait from Tsuge et al. [33]

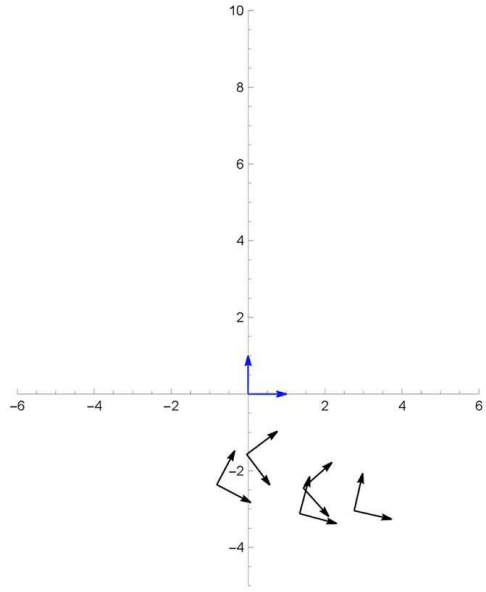

Fig. 5 Five chosen ankle poses in Example 6.1

4.3 Other Geometric Constraints. In most practical scenarios, mechanisms need to satisfy additional geometric constraints, such as limitations on the location of moving or fixed joints or sliding direction. In this subsection, we show how such constraints can also be represented using a linear equation in unknown parameters P_i, which can be combined with the aforementioned constraints to expand the design space. For example, designers may want to constrain fixed joints to lie on a given line. Additionally, a line constraint on moving joints has the ability to restrict the coupler's shape [32]. While we restrict ourselves to linear constraints only in this paper, it is worth mentioning that quadratic and other more complex constraints on joint locations can also be valuable, but more challenging in terms of computational complexity [20].

4.3.1 Geometric Constraints on Fixed and Moving Pivots. Let (X_f,Y_f) be one of the specified fixed pivot locations of an RR dyad. A line constraint for the fixed pivots requires the center point $(X_f,\ Y_f)$ of an RR dyad to lie on a line given by $K_1X_f + K_2Y_f + K_3 = 0$. From inverse kinematic relations in Eqs. (26) and (27), we know that $X_f = a_1/a_0 = P_4/2P_1$, and $Y_f = a_2/a_0 = P_5/2P_1$. Thus, the line constraint on the fixed pivot can be given by

$$K_1P_4 + K_2P_5 + 2K_3P_1 = 0 \tag{34}$$

where K_i are known. Alternatively, one can also specify the exact location of the fixed pivot by the following two linear equations

$$\begin{aligned} X_f = P_4/2P_1 \Rightarrow 2P_1X_f - P_4 = 0 \\ Y_f = P_5/2P_1 \Rightarrow 2P_1Y_f - P_5 = 0 \end{aligned} \tag{35}$$

A similar linear constraint equation for the moving pivot (x_m,y_m) constrained to lie on a line $k_1x_m + k_2y_m + k_3 = 0$ in the moving frame is given by

$$k_1P_2 + k_2P_3 + 2k_3P_1 = 0 \tag{36}$$

If the location of a moving pivot is exactly given, then we obtain linear constraint equations similar to Eq. (35)

$$\begin{aligned} x_m = P_2/2P_1 \Rightarrow 2P_1x_m - P_2 = 0 \\ y_m = P_3/2P_1 \Rightarrow 2P_1y_m - P_3 = 0 \end{aligned} \tag{37}$$

4.3.2 Geometric Constraints on Fixed and Moving Line. For an RP dyad, specifying the moving line by $k_1l_1 + k_2l_2 + k_3 = 0$ in the moving frame yields the following constraint equation:

$$k_1P_2 + k_2P_3 + 2k_3P_8 = 0 \tag{38}$$

The above follows readily from the inverse kinematic relations in Eq. (29) where $l_1 = P_2/2P_8,\ l_2 = P_3/2P_8$.

For a PR dyad, specifying the fixed sliding line by $K_1X_f + K_2Y_f + K_3 = 0$ produces another similar linear constraint given by

$$K_1P_4 + K_2P_5 = 0 \tag{39}$$

which is obtained by substituting the coordinates of the fixed pivots of an RR dyad in the equation of a line given by $K_1X_f + K_2Y_f + K_3 = 0$ and simplifying it in the limit when $a_0 = 0$.

5 Solving System of Equations Using Null Space Analysis

In this section, we present a simple two-step algorithm for satisfying five constraints in the form of Eq. (20) to obtain independent parameters of dyads. These constraints can be on a combination of pose $(d_1,\ d_2,\ \phi)$, velocity $(v,\ w,\ \dot{\phi})$, acceleration $(\dot{v},\ \dot{w},\ \ddot{\phi})$, or other geometric conditions as presented in the previous section. These constraints can be assembled to formulate a system of linear equations represented as $[A]\boldsymbol{P} = 0$, where the matrix $[A]$ is written as follows:

$$[A] = \begin{bmatrix} A_{11} & A_{12} & \cdots & A_{18} \\ A_{21} & A_{22} & \cdots & A_{28} \\ \vdots & \vdots & \ddots & \vdots \\ A_{51} & A_{52} & \cdots & A_{58} \end{bmatrix} \tag{40}$$

Table 1 Five chosen ankle poses in Example 6.1

No.	Translation	Rotation
1	(2.757, −3.043)	−12.79 deg
2	(1.339, −3.118)	−15.12 deg
3	(−0.814, −2.364)	−27.75 deg
4	(−0.037, −1.574)	−52.98 deg
5	(1.434, −2.447)	−48.33 deg

Table 2 Eigenvalues for five-pose synthesis problem in Example 6.1

612.336	9.920	4.478	0.258	0.118	5.952×10^{-14}	-3.000×10^{-15}	1.481×10^{-16}

Table 3 Eigenvectors for five-pose synthesis problem in Example 6.1

	p_1	p_2	p_3	p_4	p_5	p_6	p_7	p_8
$\boldsymbol{e}_1$	−0.0025	−0.3539	0.1995	−0.2787	0.0220	0.1187	−0.8618	0
$\boldsymbol{e}_2$	0.0282	−0.4728	0.0135	−0.3397	0.1491	0.6879	0.4057	0
$\boldsymbol{e}_3$	−0.0093	0.2810	−0.1823	0.1681	−0.0560	0.3867	−0.1601	0.8252

where A_{ij} refers to the ith task and jth Cartesian parameter in Eq. (20). In the exact synthesis problem, the system of linear equations $[A]\boldsymbol{P}$ is fully constrained. This paper uses a method called SVD to find the solution of $[A]\boldsymbol{P} = 0$. The SVD decomposes the 5×8 matrix $[A]$ into

$$[A] = [U][S][V]^T \tag{41}$$

where $[U]$ is a 5×5 unitary matrix, whose columns are the eigenvectors of $[A][A]^T$, is also called the left singular vectors of $[A]$. $[S]$ is a 5×8 non-negative real diagonal matrix whose elements are square roots of the eigenvalues of $[A][A]^T$ (or, $[A]^T[A]$). The matrix $[V]^T$ is a 8×8 unitary matrix, whose columns, called right singular vectors, are eigenvectors of $[A]^T[A]$.

The solution to $[A]\boldsymbol{P} = 0$ corresponds to the right singular vectors of the matrix $[A]$, which constitute an orthonormal basis for the null space of $[A]$. Consequently, the number of zero eigenvalues is decided by the rank of $[A]$ as $(8 - rank)$.

While $rank = 5$, the eigenvectors corresponding to the three zero eigenvalues are $\boldsymbol{e_1}$, $\boldsymbol{e_2}$, and $\boldsymbol{e_3}$, the null space can be represented by a candidate solution vector $\boldsymbol{P}$ as

$$\boldsymbol{P} = b_1\boldsymbol{e}_1 + b_2\boldsymbol{e}_2 + b_3\boldsymbol{e}_3 \tag{42}$$

where b_i are the undetermined parameters. Without any loss of generality, b_3 can be set to 1 because $\boldsymbol{P}$ is given by homogeneous coordinates. The vector $\boldsymbol{P}$ needs to satisfy the two quadratic constraints given by Eq. (25), which would lead to a degree four polynomial in a single variable. Its solution when substituted back in Eq. (42) will provide up to four solutions representing mechanical dyads.

6 Examples

In this section, we present several examples to illustrate the effectiveness of the proposed methodology. The first four examples are of designing a walk assist rehabilitation mechanism to enable disabled users to perform natural walking movements. In each of these examples, we present different sets of design constraints. Finally, we show an example with three task positions and two specified velocities and compare our results with Robson and McCarthy [27].

Table 4 Four solutions of the five-pose synthesis problem in Example 6.1

	b_1	b_2
1	−0.5941	0.2507
2	0.1868	0.3340
3	0.5618	−0.2670
4	0.0355	0.4187

6.1 Five-Pose Motion Synthesis. In this example, we seek to design a rehabilitation mechanism that can generate the essential motion of a human's typical gait pattern during walking. A set of poses are collected from human ankle motion during walking from the simulation of the six-bar mechanism designed by Tsuge et al. [33]. While Tsuge et al. designed a six-bar mechanism for ankle path generation, we are solving a motion synthesis problem, where we want to achieve specific orientations along the path. Figure 4 shows 60 prescribed poses generated along a gait cycle. For this example, five poses are chosen and shown in Fig. 5 and presented in Table 1. These five poses were selected to capture the extreme positions of the gait cycle. Nevertheless, there was some trial and error involved in selecting these poses for a better demonstration. The method discussed in this paper is only suitable for exact motion synthesis. According to Refs. [19,34], approximate synthesis is necessary for more than five poses.

Substituting the pose parameters into Eqs. (20) and (22), we get a 5×8 matrix $[A]$ as

$$[A] = \begin{bmatrix} -16.861 & -3.362 & 2.357 & 2.757 & -3.043 & -0.221 & -0.975 & 1 \\ -11.515 & -2.106 & 2.661 & 1.339 & -3.118 & -0.261 & -0.965 & 1 \\ -6.251 & -0.380 & 2.471 & -0.814 & -2.364 & -0.466 & 0.885 & 1 \\ -2.479 & -1.234 & 0.977 & -0.037 & -1.574 & -0.798 & -0.602 & 1 \\ -8.044 & -2.781 & 0.556 & 1.434 & -2.447 & -0.747 & 0.665 & 1 \end{bmatrix} \tag{43}$$

After applying the SVD to $[A]$, eigenvalues are obtained and listed in Table 2. From the results, the last three eigenvalues can be considered zero. The eigenvectors corresponding to these eigenvalues are listed in Table 3.

Substituting eigenvectors in Eq. (42), and solving for b_1 and b_2 from Eq. (25) using NSolve function in the WOLFRAM MATHEMATICA, we get four real solutions listed in Table 4 and four sets of $\boldsymbol{P}_i$ are obtained and listed in Table 5.

By observing the second row of Table 5, we see that the values of P_1, P_4, and P_5 are closer to zero than any other values. This implies the second result is closer to a RP dyad than an RR dyad. By choosing two dyads at a time, we can form six

Table 5 Parameters P_i for the five-pose synthesis problem in Example 6.1

	P_1	P_2	P_3	P_4	P_5	P_6	P_7	P_8
1	−0.003	−0.040	−0.051	−0.069	−0.005	0.529	−0.479	0.694
2	0.0001	0.049	−0.131	0.0007	0.0005	0.601	−0.169	0.768
3	−0.015	0.177	−0.063	0.087	−0.071	0.229	−0.639	0.701
4	0.002	0.065	−0.156	0.015	0.007	0.626	−0.019	0.761

Table 6 Four groups of design parameters for the five-pose synthesis problem in Example 6.1

Type	$\{x_1,\ l_1\}$	$\{x_2,\ l_2\}$	$\{x_3,\ l_3\}$	a_0	a_1	a_2	a_3
RR	6.366	8.045	1.00	1.00	11.020	0.736	−57.420
RP	0.032	−0.085	1.00	0.00	3.615	2.641	—
RR	−5.713	2.022	1.00	1.00	−2.801	2.285	−4.252
RR	14.875	−35.757	1.00	1.00	3.371	1.525	923.974

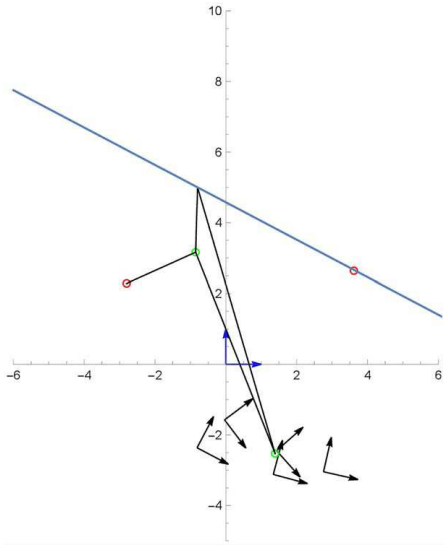

Fig. 6 RRPR mechanism from MATHEMATICA in Example 6.1

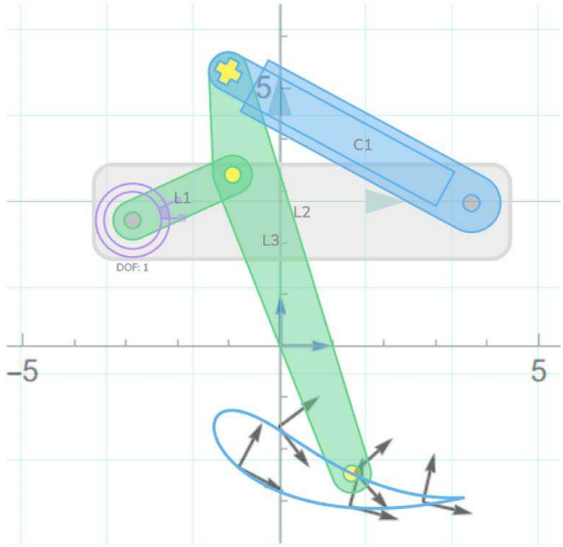

Fig. 7 RRPR mechanism from MOTIONGEN in Example 6.1

Table 7 Eigenvalues for four-pose and one-fixed joint constraint synthesis problem in Example 6.2

575.333	14.871	5.682	0.894	0.0040	3.310×10^{-14}	-9.813×10^{-15}	-1.239×10^{-15}

Table 8 Parameters P_i of the four-pose and one-fixed joint synthesis problem in Example 6.2

	P_1	P_2	P_3	P_4	P_5	P_6	P_7	P_8
1	−0.017	0.114	−0.150	0.005	−0.121	0.388	−0.556	0.700
2	0	0.049	−0.131	0	0	0.602	−0.164	0.769
3	−0.002	0.0383	−0.124	−0.013	−0.011	0.587	−0.243	0.761
4	−0.004	−0.032	−0.077	−0.072	−0.023	0.543	−0.457	0.695

four-bar mechanisms. Solving for the Cartesian parameters of each RR dyad from Eqs. (26) and (27) (RP dyad from Eqs. (29) and (30)), the final solution set is shown in Table 6. An RRPR mechanism formed by the second and third solutions is illustrated in Figs. 6 and 7. Mechanism figures shown below are drawn in MOTIONGEN [21,22] available.[4] The result for RP dyad has a small error because P_1, P_4, and P_5 are close to zero, but not exactly zero. This also explains why even though an RP dyad can go through only four poses exactly, a reinterpretation of an RR dyad as an RP dyad gives rise to an approximate synthesis only. The RR dyads only have numerical calculation errors as an exact motion synthesis problem. While it may be hard to select the best choice among all six mechanisms merely on the basis of interpolating all the five poses, in practice, one would choose the final kinematic design that avoids assembly

[4]See Note 2.

Table 9 Four groups of design parameters for the four-pose and one-fixed joint synthesis problem in Example 6.2

Type	$\{x_1,\ l_1\}$	$\{x_2,\ l_2\}$	$\{x_3,\ l_3\}$	a_0	a_1	a_2	a_3
RR	−3.389	4.467	1.00	1.00	−0.144	3.604	−5.147
RP	0.032	−0.085	1.00	1.00	3.606	2.603	—
RR	−10.778	34.899	1.00	1.00	3.771	3.128	452.707
RR	3.538	8.662	1.00	1.00	8.073	2.604	−33.938

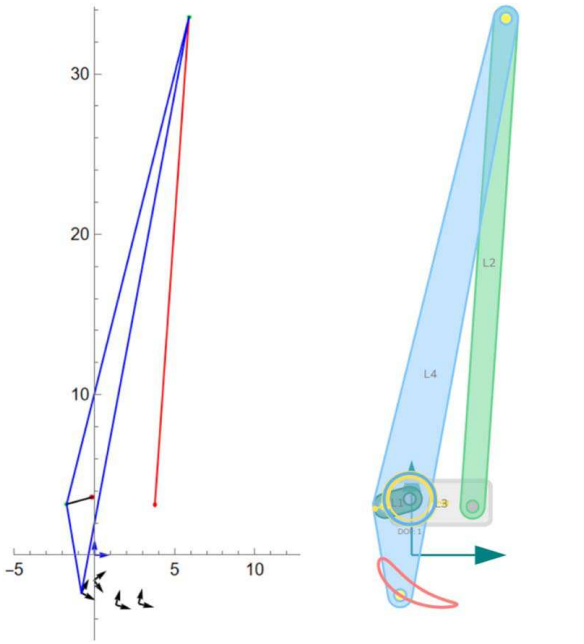

Fig. 8 RRRR mechanism from MATHEMATICA (left) and MOTIONGEN (right) in Example 6.2

mode defect, branching, and order defects with acceptable transmission angle, among others.

6.2 Four-Pose Motion Synthesis With an Extra Constraint. With the same example as above, one extra constraint on fixed joints may be desired to be located at the height of the thigh as a lower limb rehabilitation device. To add this extra constraint, the fifth pose is removed and a new constraint is added for the fixed joints to lie on a horizontal line $-0.1217a_1 - a_2 + 7.1732 = 0$ located at the height of the thigh.

We substitute the four task poses into Eqs. (20) and (22) and the extra constraint in Eq. (44) to form a 5×8 matrix $[A]$.

$$-0.1217P_4 - P_5 + 7.1732P_1 = 0 \tag{44}$$

After applying the SVD to $[A]$, eigenvalues are obtained and listed in Table 7. Once again, the last three eigenvalues are close to zero.

Following the same procedure as in the previous example, four solutions are obtained and listed in Tables 8 and 9. Among the four solutions, the second solution is close to an RP dyad and the rest are all RR dyads. The first and third solutions are chosen to form an RRRR mechanism as shown in Fig. 8. Both the fixed joints are on a given constraint line; however, the mechanism suffers from a poor link ratio. Incidentally, the RRRR mechanism with first and fourth dyad has assembly mode defects, which remains an outstanding problem [35].

Table 10 Three chosen poses and two velocities in Example 6.3

No.	Translation	Rotation	Linear velocity	Angular velocity
1	(2.757, −3.043)	−12.79 deg	(−0.155, 0.033)	−0.007 rad/s
2	(−0.814, −2.364)	−27.75 deg	(−, −)	—
3	(−0.037, −1.574)	−52.98 deg	(0.209, −0.024)	0.014 rad/s

Table 11 Parameters P_i of the three-pose with two-velocity synthesis problem in Example 6.3

	P_1	P_2	P_3	P_4	P_5	P_6	P_7	P_8
1	−0.006	−0.020	−0.010	0.019	0.311	0.535	0.220	0.753
2	−0.003	0.024	−0.063	−0.022	−0.071	0.450	−0.576	0.675
3	−0.003	0.067	−0.043	0.022	−0.053	0.402	−0.579	0.703
4	−0.004	−0.029	−0.077	−0.069	−0.025	0.541	−0.460	0.696

Table 12 Four groups of design parameters for the three-pose with two-velocity synthesis problem in Example 6.3

Type	$\{x_1,\ l_1\}$	$\{x_2,\ l_2\}$	$\{x_3,\ l_3\}$	a_0	a_1	a_2	a_3
RR	1.674	0.807	1.00	1.00	1.523	−25.406	−59.817
RR	−3.479	9.160	1.00	1.00	3.22	10.418	−50.728
RR	−10.317	6.620	1.00	1.00	−3.390	8.162	−33.016
RR	3.350	9.039	1.00	1.00	8.106	2.958	−35.080

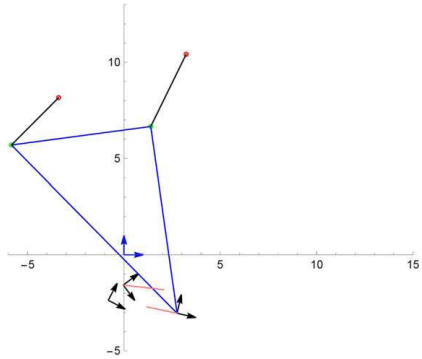

Fig. 9 RRRR mechanism from MATHEMATICA (the line segments of poses indicate velocity) in Example 6.3

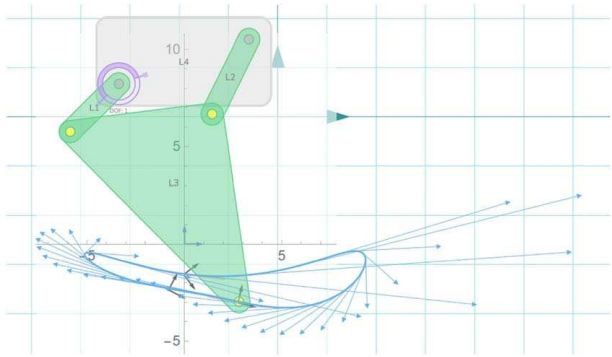

Fig. 10 RRRR mechanism drawn in MOTIONGEN with velocity vectors shown along the path

Table 13 Three chosen poses with velocity and acceleration in Example 6.4

No.	Translation	Rotation	Velocity(/, /, rad/s)	Acceleration(/, /, rad/s^2)
1	(2.757, −3.043)	−12.79 deg	(–, –, –)	(–, –, –)
2	(−0.814, −2.364)	−27.75 deg	(–, –, –)	(–, –, –)
3	(−0.037, −1.574)	−52.98 deg	(2.09, −0.24, 0.14)	(0.38, −0.21, 0.02)

Table 14 Parameters P_i of the three-pose with velocity and acceleration synthesis problem in Example 6.4

	P_1	P_2	P_3	P_4	P_5	P_6	P_7	P_8
1	0.028	−0.253	0.078	−0.125	0.058	−0.089	0.649	−0.694
2	−0.025	−0.033	−0.185	−0.150	−0.134	0.469	−0.593	0.594
3	0.002	0.020	−0.017	0.008	0.073	0.520	−0.338	0.780
4	−0.008	−0.050	−0.099	−0.010	−0.018	0.567	−0.423	0.691

Table 15 Four groups of design parameters for the three-pose with velocity and acceleration synthesis problem in Example 6.4

Type	$\{x_1,\ l_1\}$	$\{x_2,\ l_2\}$	$\{x_3,\ l_3\}$	a_0	a_1	a_2	a_3
RR	−4.540	1.393	1.00	1.00	−2.247	1.043	−1.192
RR	0.655	3.699	1.00	1.00	3.00	2.665	−4.783
RR	6.520	−5.330	1.00	1.00	2.562	23.458	285.2
RR	3.148	6.239	1.00	1.00	6.297	1.107	−19.260

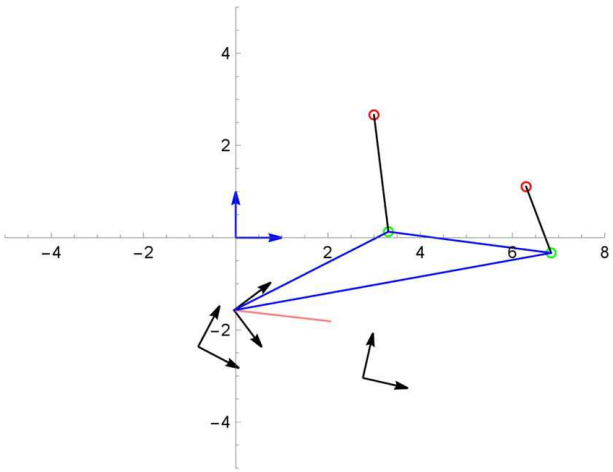

Fig. 11 RRRR mechanism from MATHEMATICA (the line segment of pose indicates velocity) in Example 6.4

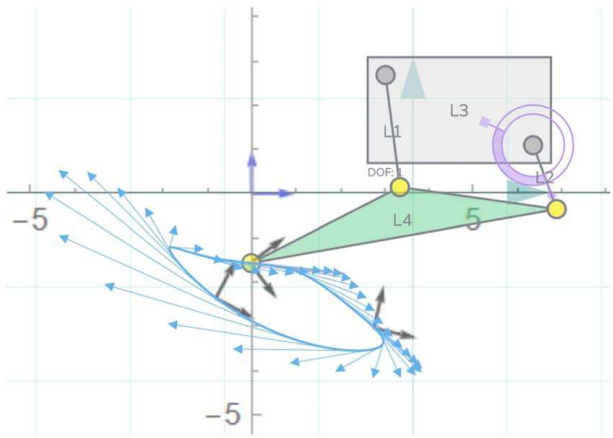

Fig. 12 RRRR mechanism from MOTIONGEN with velocity and acceleration constraints in Example 6.4

Table 16 Three chosen poses and velocities from Robson and McCarthy [27]

No.	Translation	Rotation	Linear Velocity	Angular Velocity
1	(3, 1)	0 deg	(0.3, 1)	1 rad/s
2	(1, 4)	45 deg	(–, –)	—
3	(−1, 3)	90 deg	(−0.3, 1)	−0.5 rad/s

Table 17 Four groups of design parameters for comparison in Example 6.5

Type	$\{x_1,\ l_1\}$	$\{x_2,\ l_2\}$	$\{x_3,\ l_3\}$	a_0	a_1	a_2	a_3
RR	−3.739	−1.100	1.00	1.00	0.347	0.456	0.580
RR	−2.528	0.347	1.00	1.00	−0.664	1.382	−0.529
RR	−2.033	−2.279	1.00	1.00	1.401	−0.194	−0.319
RR	11.637	−0.614	1.00	1.00	1.282	1.352	87.896

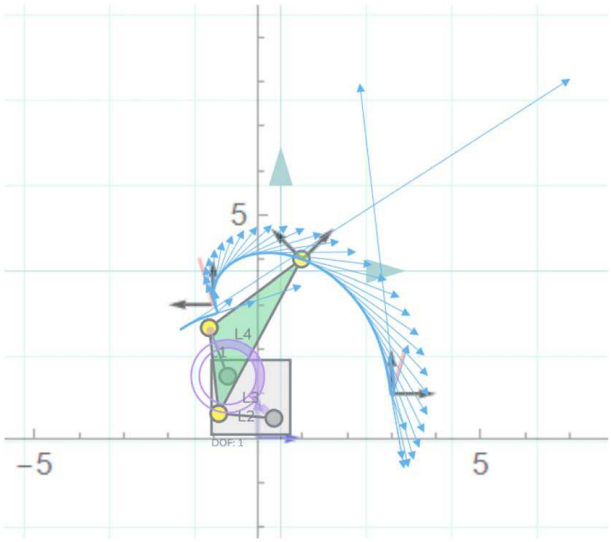

Fig. 13 An RRRR mechanism from Robson and McCarthy (the line segment of pose indicates velocity)

6.3 Motion Synthesis With Velocity Constraints. In the application of rehabilitation mechanisms, achieving velocity and acceleration similar to natural walking motion is desirable. To address this, we first introduce two-velocity constraints to the first and fourth poses in Example 6.1, while omitting the second and fifth poses. The configurations with three poses and two-velocity constraints are shown in Table 10.

The only deviation from pure pose synthesis lies in the incorporation of extra velocity constraints into Eq. (20), utilizing the A_i parameters from Eq. (23) (or Eq. (32) for RP and PP dyads). We present the resultant parameter P_i and the final four solutions directly in Tables 11 and 12. The RRRR mechanism formed by the second and third solutions is illustrated in Figs. 9 and 10.

6.4 Motion Synthesis With Velocity and Acceleration Constraints. Now we add velocity and acceleration constraints to the previous example. With the same three chosen poses in Sec. 6.3, the third pose is constrained by additional velocity and acceleration, as shown in Table 13.

While the other design equations encode the information about poses and velocity, the design equation for acceleration includes A_i parameters derived from the acceleration constraint in Eq. (24).

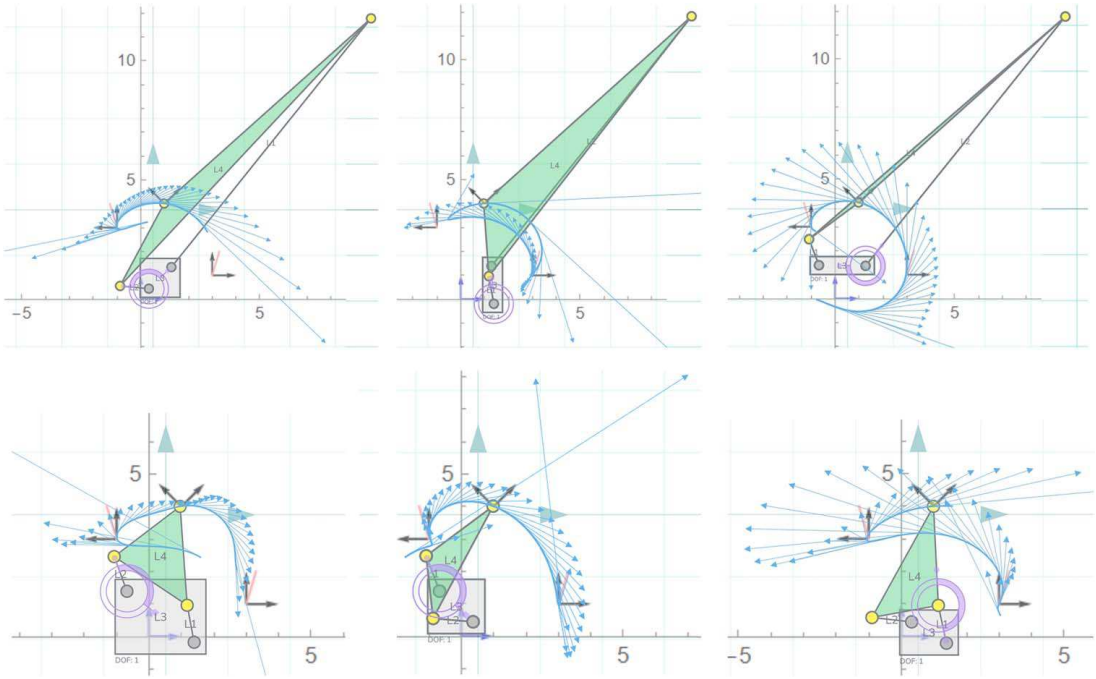

Fig. 14 Six RRRR mechanisms from our algorithm

The solving process follows the same steps as in previous examples. For brevity, we only provide the solution of parameter P_i and the final four solutions in Tables 14 and 15. The second and fourth solutions exemplify one of the RRRR mechanisms, as illustrated in Figs. 11 and 12.

6.5 Motion Synthesis With Velocity Constraints: A Comparison With Robson and McCarthy. Robson and McCarthy presented a motion synthesis method of four-bar mechanisms with three task positions and two specified velocities [27]. To validate our method, we input their data into our equations and perform a comparative analysis. The corresponding data are provided in Table 16. While they obtained only one four-bar mechanism (two RR dyads), we identified a total of six four-bar mechanisms from four dyads. The first two dyad solutions shown in Table 17 are common to both our methods. The third and fourth are the two extra solutions obtained by our method. Figure 13 shows an RRRR mechanism from Robson and McCarthy and Fig. 14 shows all six possible RRRR mechanisms from our algorithm. It is worth mentioning that the generated mechanism can satisfy all the exact pose and velocity constraints. However, the mechanism might only satisfy those constraints within different branches. This is a limitation of our method, which does not attempt to rectify circuit, branch, or order defects.

7 Conclusions

This paper has explored the simultaneous type and dimensional synthesis of planar four-bar linkages, considering a range of practical geometric and kinematic constraints, including position, velocity, acceleration, and pivot placements. Unlike conventional methods that follow a sequential approach to mechanism design, our approach introduces a matrix-based methodology that concurrently determines both type and dimensional attributes from provided data, emphasizing a holistic data-driven paradigm. The novel matrix-based approach presented in this paper has introduced two key contributions: the development of a unified design equation capable of handling a wide array of constraint types within planar dyads, and the introduction of an integrated algorithm for motion synthesis problems, thereby enabling the identification of all potential planar four-bar linkage mechanisms.

There are some limitations in this work that are expected to be addressed in future research. First, this work focuses only on exact synthesis with five constraints. Extending this approach to approximate problems to include more constraints is an equally important problem. Second, this work does not resolve issues related to circuit, branch, order, and other potential defects and extension to higher-order mechanisms is also a future research problem. Nonetheless, this research provides a unified and efficient approach for practical implementation that promises to simplify and enhance the synthesis process, making it more accessible and practical for a wide range of applications.

Data Availability Statement

The datasets generated and supporting the findings of this article are obtainable from the corresponding author upon reasonable request.

References

[1] Hamilton, W. R., 1853, *Lectures on Quaternions*, Hodges Smith & Co., Dublin, Ireland.
[2] Shoemake, K., 1985, "Animating Rotation With Quaternion Curves," SIGGRAPH 1985: 12th Annual Conference on Computer Graphics and Interactive Techniques, San Francisco, CA, July 22–26.
[3] McCarthy, J. M., 1990, *Introduction to Theoretical Kinematics*, The MIT Press, Cambridge, MA.
[4] Bottema, O., 1973, "On a Set of Displacements in Space," ASME J. Eng. Ind., **Series B 95**(2), pp. 451–454.
[5] Ravani, B., and Roth, B., 1983, "Motion Synthesis Using Kinematic Mappings," J. Mech. Transmiss. Autom. Des., **105**(3), pp. 460–467.
[6] Ravani, B., and Roth, B., 1984, "Mappings of Spatial Kinematics," J. Mech. Transmiss. Autom. Des., **106**(3), pp. 341–347.
[7] Bottema, O., and Roth, B., 1979, *Theoretical Kinematics*, Dover Publication Inc., New York.
[8] Bodduluri, R. M. C., and McCarthy, J. M., 1992, "Finite Position Synthesis Using the Image Curve of a Spherical Four-Bar Motion," ASME J. Mech. Des., **114**(1), pp. 55–60.
[9] McCarthy, J. M., 1983, "Planar and Spatial Rigid Body Motion as Special Cases of Spherical and 3-Spherical Motion," J. Mech. Transmiss. Autom., **105**(3), pp. 569–575.
[10] Larochelle, P. M., 1996, "Synthesis of Planar RR Dyads by Constraint Manifold Projection," ASME 1996 Design Engineering Technical Conferences and Computers in Engineering Conference, Irvine, CA, Aug. 18–22.
[11] Larochelle, P., 2000, "Approximate Motion Synthesis Via Parametric Constraint Manifold Fitting," *Advances in Robot Kinematics*, J. Lenarčič, and M. M. Stanišić, eds., Springer, Dordrecht, Netherlands, pp. 103–110.
[12] Ge, Q. J., and McCarthy, J. M., 1991, "The Algebraic Classification of the Image Curves of Spherical 4-Bar Motion," ASME J. Mech. Des., **113**(3), pp. 227–231.
[13] Ge, Q. J., and McCarthy, J. M., 1991, "Functional Constraints as Algebraic-Manifolds in a Clifford-Algebra," IEEE Trans. Rob. Autom., **7**(5), pp. 670–677.
[14] Park, F. C., 1995, "Distance Metrics on the Rigid-Body Motions With Applications to Mechanism Design," ASME J. Mech. Des., **117**(1), pp. 48–54.
[15] Larochelle, P., and McCarthy, J. M., 1995, "Planar Motion Synthesis Using an Approximate Bi-Invariant Metric," ASME J. Mech. Des., **117**(4), pp. 646–651.
[16] Xu, T., Myszka, D. H., and Murray, A. P., 2024, "A Bi-Invariant Approach to Approximate Motion Synthesis of Planar Four-Bar Linkage," Robotics, **13**(1), p. 13.
[17] Hayes, M. J. D., Luu, T., and Chang, X. W., 2004, "Kinematic Mapping Application to Approximate Type and Dimension Synthesis of Planar Mechanisms," *Advances in Robot Kinematics*, J. Lenarčič, and C.Galletti, eds., Springer, Dordrecht, Netherlands, pp. 41–48.
[18] Luu, T. J., and Hayes, M. J. D., 2012, *Integrated Type And Dimensional Synthesis of Planar Four-Bar Mechanisms* (Latest Advances in Robot Kinematics), Springer, New York.
[19] Ge, Q., Purwar, A., Zhao, P., and Deshpande, S., 2017, "A Task-Driven Approach to Unified Synthesis of Planar Four-Bar Linkages Using Algebraic Fitting of a Pencil of G-Manifolds," ASME J. Comput. Inf. Sci. Eng., **17**(3), p. 031011.
[20] Deshpande, S., and Purwar, A., 2017, "A Task-Driven Approach to Optimal Synthesis of Planar Four-Bar Linkages for Extended Burmester Problem," ASME J. Mech. Rob., **9**(6), p. 061005.
[21] Purwar, A., Deshpande, S., and Ge, Q. J., 2017, "MotionGen: Interactive Design and Editing of Planar Four-Bar Motions Via a Unified Framework for Generating Pose- and Geometric-Constraints," ASME J. Mech. Rob., **9**(2), p. 024504.
[22] Lyu, Z., Purwar, A., and Liao, W., 2024, "A Unified Real-Time Motion Generation Algorithm for Approximate Position Analysis of Planar N-Bar Mechanisms," ASME J. Mech. Des., **146**(6), p. 063302.
[23] Zhao, P., Li, X., Purwar, A., and Ge, Q. J., 2016, "A Task-Driven Unified Synthesis of Planar Four-Bar and Six-Bar Linkages With R- and P-Joints for Five-Position Realization," ASME J. Mech. Rob., **8**(6), p. 061003.
[24] Schaefer, R. S., and Kramer, S. N., 1979, "Selective Precision Synthesis of Planar Mechanisms Satisfying Position and Velocity Constraints," Mech. Mach. Theory, **14**(3), pp. 161–170.
[25] Holte, J.E., 1996, "Two Precision Position Synthesis of Planar Mechanisms with Approximate Position and Velocity Constraints," Ph.D dissertation, University of St. Thomas, Minneapolis, MN.
[26] Holte, J. E., Chase, T. R., and Erdman, A. G., 2001, "Approximate Velocities in Mixed Exact-Approximate Position Synthesis of Planar Mechanisms," ASME J. Mech. Des., **123**(3), pp. 388–394.
[27] Robson, N. P., and McCarthy, J. M., 2005, "The Synthesis of Planar 4R Linkages With Three Task Positions and Two Specified Velocities," ASME 2005 International Design Engineering Technical Conferences and Computers and Information in Engineering Conference, Volume 7: 29th Mechanisms and Robotics Conference, Parts A and B, Long Beach, CA, Sept. 24–28, pp. 425–432.
[28] Robson, N. P., McCarthy, J. M., and Tumer, I. Y., 2008, "The Algebraic Synthesis of a Spatial TS Chain for a Prescribed Acceleration Task," Mech. Mach. Theory, **43**(10), pp. 1268–1280.
[29] Robson, N., and McCarthy, J., 2009, Applications of the Geometric Design of Mechanical Linkages With Task Acceleration Specifications. Vol. 7. 10.1115/DETC2009-87415.
[30] Coxeter, H., 1974, *Projective Geometry*, 2nd ed., Springer-Verlag, New York.
[31] Stolfi, J., 1991, *Oriented Projective Geometry*, Academic Press Professional Inc., Boston, MA.
[32] Sharma, S., and Purwar, A., 2020, "Unified Motion Synthesis of Spatial Seven-Bar Platform Mechanisms and Planar-Four Bar Mechanisms," ASME 2020 International Design Engineering Technical Conferences and Computers and Information in Engineering Conference, Virtual Online, Aug. 17–19.
[33] Tsuge, B. Y., Plecnik, M. M., and Michael McCarthy, J., 2016, "Homotopy Directed Optimization to Design a Six-Bar Linkage for a Lower Limb With a Natural Ankle Trajectory," ASME J. Mech. Rob., **8**(6), p. 061009.
[34] Tsuge, B. Y., and Michael McCarthy, J., 2016, "An Adjustable Single Degree-of-Freedom System to Guide Natural Walking Movement for Rehabilitation," ASME J. Med. Devices, **10**(4), p. 044501.
[35] Chase, T. R., and Mirth, J. A., 1993, "Circuits and Branches of Single-Degree-of-Freedom Planar Linkages," ASME J. Mech. Des., **115**(2), pp. 223–230.